Journal of Magnetism and Magnetic Materials 562 (2022) 169793

Contents lists available at ScienceDirect

Journal of Magnetism and Magnetic Materials

journal homepage: www.elsevier.com/locate/jmmm

Research article

Voltage-driven multistability and chaos in magnetic films

Susana Contreras-Celada [a,*], Marcel G. Clerc [b], Saliya Coulibaly [c], René G. Rojas [a], Alejandro O. Leon [d]

[a] Instituto de Física, Pontificia Universidad Católica de Valparaíso, Casilla 4059, Chile
[b] Departamento de Física and Millennium Institute for Research in Optics, Facultad de Ciencias Físicas y Matemáticas, Universidad de Chile, Casilla 487-3, Santiago, Chile
[c] Université de Lille, CNRS, UMR 8523 - PhLAM - Physique des Lasers Atomes et Molécules, F-59000 Lille, France
[d] Departamento de Física, Facultad de Ciencias Naturales, Matemática y del Medio Ambiente, Universidad Tecnológica Metropolitana, Las Palmeras 3360, Ñuñoa 780-0003, Santiago, Chile

ARTICLE INFO

Keywords:
Voltage-controlled magnetic anisotropy
Magnetization dynamics
Landau–lifshitz equation
Nano-oscillators
Chaos
Dynamical systems

ABSTRACT

The control of magnetization dynamics has allowed numerous technological applications. Magnetization dynamics can be excited by, *e.g.*, alternating magnetic fields, charge and spin currents, and a voltage-induced control of interfacial properties. An example of the last mechanism is the voltage-controlled magnetic anisotropy effect, which can induce magnetization precessions and switchings with low-power consumption. Time-dependent voltage-controlled magnetic anisotropy can induce complex dynamic behaviors for magnetization. This work studies the magnetization dynamics of a single magnetic nano-oscillator forced with a time-dependent voltage-controlled magnetic anisotropy. Unexpectedly, the oscillator displays multistable regimes, *i.e.*, distinct initial conditions evolve towards different oscillatory states. When voltage is changed the oscillatory state exhibits period-doubling route to chaos. The chaotic behavior is numerically demonstrated by the determination of the largest Lyapunov exponent.

1. Introduction

Driven oscillators exhibit a plethora of behaviors, including chaos [1–3], synchronization [4], and chimeras [5–7]. In the case of magnetic media, the magnetization exhibits damped precessions around a net magnetic field. The injection of energy via oscillatory fields and current-induced torques can compensate for the dissipation and generate permanent states and dynamics, including self-sustained oscillations [8–10], textures [11–14], dissipative solitons [15,16], domain walls [17–20], and chaos [21–24], to mention a few. However, unfortunately, magnetic fields are generally not localized, and the Joule heating that comes along with electric currents increases the device's energy demand. An alternative driving effect is the voltage-controlled magnetic anisotropy (VCMA) [25–34]. In the simplest instance of a VCMA, a voltage at a metallic|insulating interface modulates the perpendicular magnetic anisotropy of the system. Because of the insulating barrier, the VCMA effect is a localized excitation that avoids Joule heating. Using a time-dependent voltage, the VCMA effect can switch the magnetization from one equilibrium to another [25,28,34], making it a low-power consumption candidate to magnetic memory writing. Furthermore, it can also induce ferromagnetic [27,29] and parametric resonances [35–41]. From the point of view of dynamical systems theory, the VCMA affects the coefficient of linear and nonlinear effective forces at the onset of resonances and instabilities [42], generating unexpected states. Therefore, a set of voltage-controlled magnetic nano-oscillators could be an ideal system for studying collective behaviors [43]. On the other hand, characterizing the dynamics of a single voltage-driven magnet may provide the vital information required to understand several interacting units. Hence, the purpose of this article is to address the dynamics of a single voltage-driven magnetic oscillator.

Via the numerical integration of the Landau–Lifshitz (LL) equation [10], we study a uniform magnetic nano-oscillator driven by a harmonic voltage in the presence of an constant magnetic field. Because of the voltage, the effective field associated to the perpendicular-magnetic-anisotropy becomes a time-dependent function which, at linear order in the small magnetization components, is equivalent to a localized oscillatory magnetic field. As a result of the energy injection, the magnetization exhibits a family of oscillatory states. The simplest oscillatory state has the same period of the forcing voltage. Increasing the voltage amplitude, this state becomes unstable and gives rise to an oscillation with twice the driving period, *i.e.,* the system responds at a half of the forcing frequency. This instability regularly repeats for

* Corresponding author.
E-mail address: susana.contreras@pucv.cl (S. Contreras-Celada).

https://doi.org/10.1016/j.jmmm.2022.169793
Received 3 June 2022; Received in revised form 3 August 2022; Accepted 4 August 2022
Available online 8 August 2022

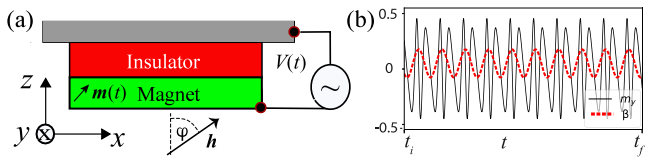

Fig. 1. Schematic setup and dynamics of a VCMA-driven nano-oscillator. (a) An insulator|metal interface is subject to a voltage, producing an excess or deficit of electrons in this region, which in turn modulates the perpendicular-magnetic-anisotropy (PMA) coefficient β. The presence of a tilted constant magnetic field $\mathbf{h}$ makes the PMA-field (*i.e.,* the field proportional to β) equivalent to a voltage-dependent magnetic field that can excite the magnetization in a localized and energy-efficient way. On the other hand, when $\mathbf{h}$ points along the z-axis, *i.e.,* $\varphi = 0$, the torque by the PMA-field is proportional to the small m_x and m_y magnetization components and a parametric-type phenomenology is observed [41]. Thus, we focus on the $\varphi > 0$ case. (b) The chart shows the temporal evolution of the PMA coefficient $\beta(t)$ and the magnetization component $m_y(t)$, respectively, for a small voltage amplitude. As this figures illustrates, the magnetization component m_y oscillates with the same periodicity of β. The oscillation of m_x (not shown) is similar to that of m_y, while m_z is almost-saturated around 1 due to the norm conservation property, $m_z = \sqrt{1 - m_x^2 - m_y^2}$, for small β_1 values. We used $\beta_1 = 0.126$, $t_i = 92000$, and $t_f = 92800$.

larger voltages, leading to a chaotic state; this scenario is referred to as the *period-doubling route to chaos* [1,2]. In this bifurcation cascade, we unveil an unexpected region of multistability, *i.e.,* a zone where two or more different stable precessional states coexist. Hence, depending on the initial condition, the magnetization can reach different steady states or attractors [2]. Namely, the system exhibits different states that could produce new functionalities of the driven nano-oscillator or induce rich collective dynamics in oscillator arrays. We numerically characterize the oscillatory states and their corresponding bifurcation diagrams. In addition, we monitor the largest Lyapunov exponent (LLE) [44], which characterizes the exponential sensibility to the initial conditions. A positive exponent demonstrates the presence of chaos in the system. Since this type of VCMA-driven oscillator is proposed as a unit of magnetic networks, we expect that the found multistability may play a role in forming collective behaviors, such as front propagation and chimeras [5–7].

2. Model and methods

The magnetization trajectories evolve on a spherical surface [10] according to the following equation, known as the Landau–Lifshitz (LL) model [10], that we write in its dimensionless form

$$\dot{\mathbf{m}} = -\mathbf{m}\times\mathbf{h}_{\text{eff}} - \alpha\mathbf{m}\times(\mathbf{m}\times\mathbf{h}_{\text{eff}}), \qquad (1)$$
$$\mathbf{h}_{\text{eff}} = \mathbf{h} + \beta m_z \mathbf{e_z},$$

where $\mathbf{m}(t) = m_x\mathbf{e_x} + m_y\mathbf{e_y} + m_z\mathbf{e_z}$ is the normalized magnetization, $\{\mathbf{e_x}, \mathbf{e_y}, \mathbf{e_z}\}$ are the Cartesian unit vectors, z-axis is the perpendicular-to-plane direction (Cartesian axes are depicted in Fig. 1), and $\mathbf{m}(t)$ depends on the dimensionless time t. Disregarding the spacial dependence of the magnetization – *the macrospin approximation* – is appropriate for media of lateral dimensions of about 100 nm or smaller. The symbols $\times$ and $\dot{\mathbf{m}}$ stand for the cross product and the derivative of $\mathbf{m}$ with respect to t, respectively. The effective magnetic field on the magnetization is $\mathbf{h}_{\text{eff}}$ and it has contributions from the external magnetic field, $\mathbf{h} = h\left[\cos(\varphi)\,\mathbf{e_z} + \sin(\varphi)\,\mathbf{e_x}\right]$, and the perpendicular-magnetic-anisotropy (PMA) field, $\beta m_z\mathbf{e_z}$ [*cf.* Fig. 1(a)]. Magnetic films have PMA due to their shape and to spin–orbit coupling [45]. Also, the sign and magnitude of the PMA coefficient β can be tuned by controlling the thickness of thin magnetic films. Another control mechanism applies when the magnet is part of an insulator|metal interface. While a voltage in a fully metallic structure generates a charge flow, an insulating barrier prevents the formation of charge currents and therefore eliminates the current-dependent Joule dissipation. In this scenario, the voltage creates charge accumulation and deficit at the insulator's opposing interfaces, *i.e.,* the screening effect occurs. This screening generates an anisotropic shift of the electrostatic energy between a magnetic interfacial atom and the screening layer. In atoms with substantial spin–orbit coupling, *e.g.,* most rare earths, there is a robust locking between their 4f charge and spin densities, which allows parametrizing the voltage-generated electrostatic energy by the atomic spins [31,32]. On the other hand, transition metals, such as Co or Fe films, have a much weaker spin–orbit interaction. In this case, the voltage-induced charge density modifies the populations of states, which then affects several properties, including the PMA (see Ref. [33] and references therein). Then, a voltage makes the β coefficient a control parameter. Since these effects take place at the interface, its relative importance increases when the magnetic medium is very thin, with some films reaching sub-nanometer thicknesses [33]. In what follows, we focus on an oscillatory voltage with a PMA coefficient given by

$$\beta = \beta_0 + \beta_1\cos(\omega t), \qquad (2)$$

with ω the forcing angular frequency, β_0 and β_1 account for the constant and oscillatory anisotropy coefficients, respectively. The latter having the general form $\beta_1 = \epsilon_V V_{\text{osc}}/\epsilon_0$, where ϵ_V is the coupling energy per unit of voltage [31], and it accounts for the VCMA energy. ϵ_V is material-dependent, and V_{osc} is the oscillatory component of the voltage; the reference energy is $\epsilon_0 = \mu_0 M_s^2 V_0$ typically the shape anisotropy with M_s the saturation magnetization, *i.e.,* its norm, and V_0 is the magnet's volume. Therefore, the β_1 coefficient accounts for the competition between the VCMA coupling energy and the energy scale at the bulk.

The second term of Eq. (1) is the damping torque and it is ruled by the dimensionless constant α. Note that this Rayleigh-type dissipation vanishes at equilibrium $\dot{\mathbf{m}} = 0$, as expected. The most prominent dissipation source is the spin–orbit coupling that induces mechanical excitation from a dynamic magnetization. Even for materials with low spin–orbit coupling, there are several dissipation channels in magnetic systems, including spin- and phonon-pumping.

When there is no energy injection, $\beta_1 = 0$, and the damping constant α is also zero, the magnetization exhibits counterclockwise precessions around $\mathbf{h}_{\text{eff}}$. On the other hand, for $\alpha > 0$ and $\beta_1 = 0$, the magnetization damps its motion until becoming parallel to $\mathbf{h}_{\text{eff}}$. Thus, the role of the oscillatory voltage is to excite permanent magnetization motions. For a finite β_1, there are two main dynamical responses. First, when the external field points along the z-axis [$\varphi = 0$ in Fig. 1(a)], the dynamics of the oscillation amplitude has a forcing term that is proportional to β_1 and to the amplitude itself, that is, the nano-oscillator is a parametric resonator [46] and oscillates at a half of the forcing frequency. In this limit, parametric instabilities appear [35–40] and, for large-enough magnets, complex nonuniform structures emerge [41]. On the other hand, when $\mathbf{h}$ is not parallel to the z-axis (*i.e.,* $\varphi \neq 0$), the forcing acting on the oscillation amplitude depends exclusively on time, except by (smaller) higher-order corrections. That is, the driving mechanism becomes independent of the oscillation amplitude. The PMA field is approximately equivalent to a localized and energy-efficient oscillatory external field in this regime. Hence, when $\beta_1 \neq 0$ and $\varphi \neq 0$, the VCMA gives rise to the usual ferromagnetic resonance for small β_1 values, resulting in a magnetization oscillation at the voltage frequency, as shown in Fig. 1(b). When β_1 is increased, a set of bifurcations occurs, as discussed in the next section.

The differential equation (1) is nonlinear and has time-varying coefficients. This type of equation has simple analytic solutions only in a few limited cases. Hence, the most appropriate and systematic strategy to understand the dynamics is through numerical studies. We employ a fourth-order Runge–Kutta algorithm with a constant step size $\Delta t = T/500$ for the numerical integration, with $T = 2\pi/\omega$ being the forcing period. We use $\omega = 0.08$ and then $\Delta t \approx 0.157$. Each simulation starts from an initial condition and relaxes for a time $t_0 = 1200T \sim \mathcal{O}(10^5)$, which is long enough to obtain the steady-state dynamics. Other parameters are $\varphi = 0.3$, $h = 0.1$, $\alpha = 0.005$, and $\beta_0 = 0.05$. We

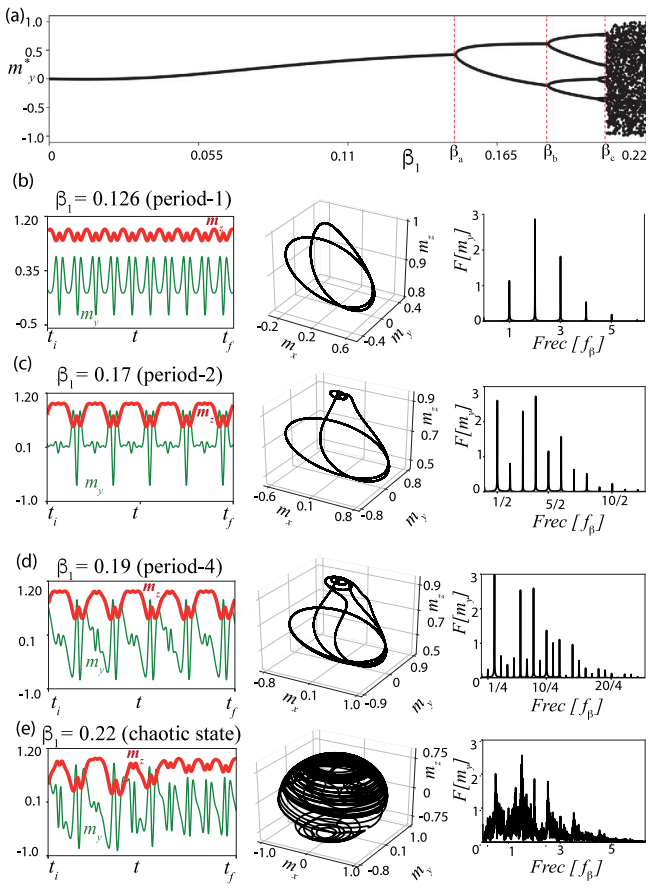

Fig. 2. Voltage-induced oscillatory states in a nano-oscillator. (a) The bifurcation diagram is a stroboscopic map $m_y^* = \{m_y(t_0 + mT) | \quad m \in \mathbb{N}\}$ of the magnetization component m_y after a transient time (t_0), *i.e.,* for each β_1 value, m_y is plotted every $T = 2\pi/\omega$ time units. Orbits with period T appear as a single point because $m_y(t+T) = m_y(t)$. We call them period-1 states. Other periodic orbits repeat every mT time units, $m_y(t + mT) = m_y(t)$, with m an integer. These are the period-m solutions. (b) Period-1 limit cycle that oscillates at the period of the forcing voltage and obtained for $\beta_1 = 0.126$. The left panel is the m_y and m_z trajectories. m_x is similar to m_y and provides no additional information, and therefore it is not shown. The central panel shows the temporal evolution in three dimensions, $(m_x, m_y, m_z)(t)$; and, finally the right panel accounts for the Fourier amplitude in arbitrary units with frequency in units of the forcing frequency $f_\beta = \omega/(2\pi)$. Note that the fundamental frequency (peak with the smaller frequency) is equal to f_β. (c) Period-2 state for $\beta_1 = 0.17$. As the Fourier plot illustrates, the fundamental frequency is a half of the forcing one, and then the system responds doubling the period. (d) Period-4 state for $\beta_1 = 0.19$ that oscillates with fundamental frequency $f = f_\beta/4$. (e) The chaotic state for $\beta_1 = 0.22$. While the Fourier spectrum of periodic orbits is discrete, the chaotic one is continuum. We used $t_i = 92000$ and $t_f = 92800$, and the three-dimensional plots (middle panel) of (b), (c), (d), and (e) show the magnetization trajectory for a duration of 3252 time units.

used the Cartesian representation of the magnetization, and the three components m_x, m_y, and m_z were integrated. We monitor the constraint of unit magnetization norm, $|\mathbf{m}(t)| = 1$, which is fully satisfied.

We integrate Eq. (1) and present our results using dimensionless quantities. However, to recover the units of the magnetization, time, and effective field, we multiply by M_s, $t_c = (\gamma M_s)^{-1}$, and $\mu_0 M_s$, respectively, where γ is the modulus of the gyromagnetic ratio and the characteristic time t_c is usually in the scale of picoseconds for $M_s \sim 10^6$ A/m.

3. Bifurcation diagram and characterization of the simplest oscillatory states

An oscillatory voltage can induce a resonance in the magnet when the forcing frequency is similar to the magnet's natural frequency. This case is illustrated in Fig. 1(b), which plots both the perpendicular-to-plane anisotropy coefficient $\beta(t) = \beta_0 + \beta_1 \cos(\omega t)$ and the response of the magnetization component $m_y(t)$. Both variables oscillate with the same period $T = 2\pi/\omega$, as expected. We call this state period-1 solution. The periodicity of the magnetization allows one to use a stroboscopic map where, for a fixed β_1, one collects a set of magnetization values measured at times $t = t_0 + mT$, m being an integer. The result of this stroboscopic map is shown in Fig. 2(a) for several β_1 values. We use a *continuation method,* where the final state of the system obtained for a β_1 value is the initial condition for another value of β_1. The difference between two consecutive β_1 values is in the range $10^{-5} - 10^{-4}$. The period-1 state appears in Fig. 2(b), where the left panel shows the magnetization components m_y and m_z as a function of time, and m_x is not shown due to its similarity with m_y. While m_y and m_x exhibit oscillations around zero, the m_z component is almost saturated and becomes a slave variable due to the norm conservation, $m_z = \sqrt{1 - \left(m_x^2 + m_y^2\right)}$. The center panel is $\mathbf{m}(t)$ in the Cartesian representation. The trajectory is a closed orbit with two well-defined m_y minima in each cycle. The Fourier transform of m_y, $F\left(m_y\right)$, is characterized by a fundamental frequency that is equal to the forcing one, $f_\beta = \omega/(2\pi)$. Additional Fourier peaks are harmonics of the fundamental frequency and emerge due to the nonlinear nature of the system, *i.e.,* the nonlinearities couple different modes [2]. When the $\beta_1 = \beta_a = 0.1505$, the system undergoes a *period-doubling bifurcations* [2], giving rise to the state shown in Fig. 2(c). This is the period-2 state (its period is $2T$) and spends a considerable amount of time near the $m_z = 1$ point of the unit sphere. We can notice that the three-dimensional orbit is modified to display a more complex trajectory around the north pole and the Fourier spectrum now has a fundamental frequency equal to $f_\beta/2$ and presents more harmonics. Likewise, for $\beta_1 = \beta_b = 0.184$, the period-2 state becomes unstable and a period-4 solution appears [*cf.* Fig. 2(d)]. Each one of these instabilities leads to a new state with twice the period of the previous cycle. A cascade of period-doubling bifurcations usually ends in a chaotic state [see Fig. 2(e)]. Indeed, the driven nano-oscillator presents a period-doubling route to chaos [1,2]. This is also the case of the present magnetic system, where chaos is observed for $\beta_1 \geq \beta_c = 0.2055$. A chaotic solution is characterized by being aperiodic and exhibits exponential sensibility to the initial conditions. The last property is characterized by the largest Lyapunov exponent (LLE) [44], $\lambda_{\mathrm{LLE}} = \lim_{t\to\infty} t^{-1} \ln(|\delta\mathbf{m}(t)|/|\delta\mathbf{m}(0)|)$, where $\delta\mathbf{m}$ is the difference between two magnetization trajectories that were initially close, $|\delta\mathbf{m}(0)| \to 0$. The largest Lyapunov exponent provides information on permanent dynamics with exponential sensitivity to nearby initial conditions. When the largest Lyapunov exponent is negative (positive), the system has a non-chaotic (chaotic) equilibrium, respectively. A standard method for calculating λ_{LLE} is by integrating the differential equation of $\delta\mathbf{m}$, namely $\delta\dot{\mathbf{m}} = \mathbb{J}(\mathbf{m}, t) \cdot \delta\mathbf{m}$, where $\mathbb{J}$ is the Jacobian of the LL equation and it depends on the magnetization solution $\mathbf{m}(t)$ and time t. Fig. 3 shows the LLE as a function of β_1, obtained by the integration of the linear equation of $\delta\mathbf{m}$, with a single random initial condition for each β_1 value. The computation scheme observes the $\delta\mathbf{m} \cdot \mathbf{m} = 0$ condition that comes from the conservation of the magnetization norm. When the magnetization oscillates periodically, $\lambda_{\mathrm{LLE}} \sim -5 \times 10^{-4}$, *cf.* Fig. 3, which implies that nearby trajectories converge to a single attractor with a well-defined oscillatory phase. This behavior is expected in non-autonomous systems, in which the oscillation phase of the solutions is fixed by the forcing. Near the instabilities of the period-m orbits, the LLE is negative but closer to zero. On the other hand, in the chaotic region, we find a positive λ_{LLE}, with, *e.g.,* $\lambda_{\mathrm{LLE}} \sim 0.007$. We observe the abrupt emergence of chaos at $\beta_1 = \beta_c$, which resembles the crisis mechanism observed in lasers [47]. Note that the Fourier spectrum of the chaotic state is continuous, as in Fig. 2(e).

A cascade of period-doubling bifurcations may appear in several systems [2]. Indeed, this is a generic chaos emergency mechanism [1]. However, the multistability of families of cycles, each one with a

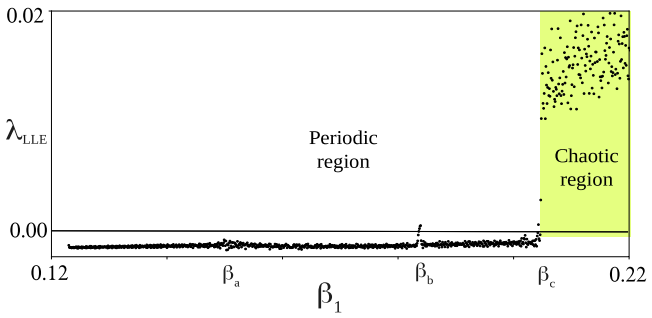

Fig. 3. Largest Lyapunov exponent (LLE), λ_{LLE}, as a function of the forcing parameter β_1. The LLE shows the exponential dependence of the initial condition. In the periodic region, $\beta_1 \leq \beta_c$, the exponent is negative, which implies that initially nearby orbits converge to a single cycle, which is a phase-locked oscillatory attractor. On the other hand, the LLE becomes positive in the chaotic zone $\beta_1 \geq \beta_c$, which describes the exponential separation of two magnetization trajectories.

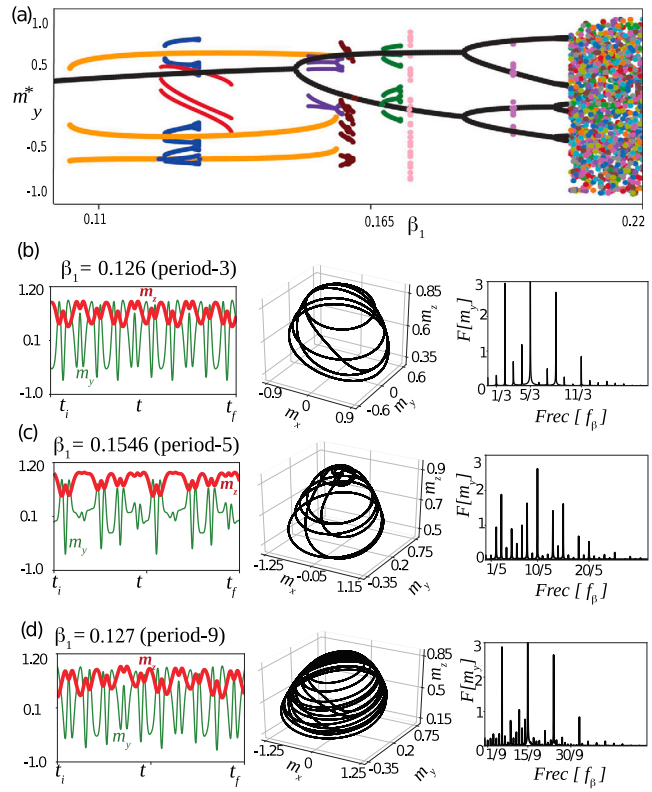

Fig. 4. Voltage-induced a family of oscillatory states. Similar to Fig. 2, but emphasizing unexpected states, such as the period-3 of small (red) and large (orange) amplitude, period-5 (dark violet), period-6 (green), period-8 (maroon), period-9 (blue) and period-16 of small (light violet) and large (pink) amplitude cycles. The black curves are the same as Fig. 2 and correspond to the period-2^n family. These solutions emerge as a monostable period-1 cycle for small β_1, that is, all initial conditions reach the same state for small enough energy injection. As this figure illustrates, there are several stable states in vast regions of the parameter space. The initial conditions are $m_x(0) = 0.650$, $m_y(0) = 0.045$, and $m_z(0) = 0.751$ for (b); $m_x(0) = 0.310$, $m_y(0) = -0.075$, and $m_z(0) = 0.948$ for (c), and $m_x(0) = -0.185$, $m_y(0) = -0.757$, and $m_z(0) = 0.627$ for (d).

set period-doubling instabilities, is less frequent. Fig. 4(a) shows a bifurcation diagram where several random initial conditions were given and their dependence on the bifurcation parameter were studied via the continuation method. Among the new oscillatory state families, we can observe two types of period-3 solutions in Fig. 4(b). This state, which has a fundamental frequency of $f_\beta/3$, is stable for the same parameter values where the period-1 solution is stable. Furthermore, depending on the initial condition, we may also reach many other equilibria, as shown in Fig. 4(a). The multistability between these four states may open opportunities when considering the dynamics of several coupled states. Fig. 4(b–c) show period-5 and period-9 solutions. There are also more fragile cycles, that are observed for a single value of the voltage amplitude, in particular, $\beta_1 = 0.173$ and $\beta_1 = 0.1938$.

4. Conclusions and remarks

Forced ferromagnets exhibit universal behaviors, including limit-cycles and chaos. Such versatility makes them ideal network units, which is promising when the forcing mechanism is a voltage in an insulating structure because of its localized effect, achieved with relatively low power consumption. On the other hand, fully characterizing the dynamics of a single voltage-driven oscillator shall provide vital information to understanding the collective behaviors of voltage-driven nano-oscillator networks. This article presents a step in that direction.

We investigated a magnetic thin film driven by an oscillatory voltage in the presence of a constant magnetic field. The film was modeled using the Landau–Lifshitz (LL) equation in the macrospin, or space-independent, approximation, valid for small lateral dimensions. Numerical integration of the LL equation revealed a cascade of period-doubling bifurcations, after which the oscillatory states divide their fundamental frequency by two. This scenario leads to a chaotic state, as demonstrated by the largest Lyapunov exponent. More intriguingly, the nano-oscillator exhibits multistability in large regions of the parameter space. Then, the magnetization can reach several attractors depending on the initial condition.

We expect this plethora of oscillatory states to motivate investigations on the magnetization switching between dynamic states in nano-oscillators, and their use as low-energy frequency converters and reservoir computing units, among other applications.

CRediT authorship contribution statement

Susana Contreras-Celada: Conceptualization, Software, Investigation. **Marcel G. Clerc:** Conceptualization, Methodology, Supervision. **Saliya Coulibaly:** Conceptualization, Methodology, Supervision. **René G. Rojas:** Conceptualization, Writing – review & editing, Supervision. **Alejandro O. Leon:** Conceptualization, Writing – original draft, Supervision.

Declaration of competing interest

The authors declare that they have no known competing financial interests or personal relationships that could have appeared to influence the work reported in this paper.

Data availability

Data will be made available on request.

Acknowledgments

This research was partially supported by Postdoctorado FONDECYT 2019 Folio 3190030, FONDECYT, Chile project 1210353, ANID-Millennium Science Initiative Program-ICN17-012 (MIRO), PROGRAMA DE COOPERACION CIENTIFICA ECOS-ANID ECOS200006 and DI INVESTIGACION INNOVADORA INTERDISCIPLINARIA PUCV 2021 No 039.409/2021. Nanoionica: Un enfoque interdisciplinario. SC acknowledges the program ECOS-Sud C20E07.

References

[1] J. Guckenheimer, P. Holmes, Nonlinear Oscillations, Dynamical Systems, and Bifurcations of Vector Fields, Springer, New York, 1983, http://dx.doi.org/10.1007/978-1-4612-1140-2.

[2] S.H. Strogatz, Nonlinear Dynamics and Chaos:With Applications to Physics, Biology, Chemistry, and Engineering, Westview Press, 2001.

[3] E. Ott, Chaos in Dynamical Systems, Cambridge University Press, 2002, http://dx.doi.org/10.1017/CBO9780511803260.

[4] A. Pikovsky, M. Rosenblum, J. Kurths, Synchronization: A Universal Concept in Nonlinear Sciences, Cambridge University Press, 2001, http://dx.doi.org/10.1017/CBO9780511755743.

[5] Y. Kuramoto, D. Battogtokh, Coexistence of coherence and incoherence in nonlocally coupled phase oscillators, Nonlinear Phenom. Complex Syst. 5 (2002) 380.

[6] D.M. Abrams, S.H. Strogatz, Chimera states for coupled oscillators, Phys. Rev. Lett. 93 (2004) 174102, http://dx.doi.org/10.1103/PhysRevLett.93.174102.

[7] M.G. Clerc, S. Coulibaly, M.A. Ferré, M.A. García-Ñustes, R.G. Rojas, Chimera-type states induced by local coupling, Phys. Rev. E 93 (2016) 052204, http://dx.doi.org/10.1103/PhysRevE.93.052204.

[8] S.I. Kiselev, J.C. Sankey, I.N. Krivorotov, N.C. Emley, R.J. Schoelkopf, R.A. Buhrman, D.C. Ralph, Microwave oscillations of a nanomagnet driven by a spin-polarized current, Nature 425 (2003) 380, http://dx.doi.org/10.1038/nature01967.

[9] A. Slavin, V. Tiberkevich, Nonlinear auto-oscillator theory of microwave generation by spin- polarized current, IEEE Trans. Magn. 45 (2009) 1875, http://dx.doi.org/10.1109/TMAG.2008.2009935.

[10] I.D. Mayergoyz, G. Bertotti, C. Serpico, Nonlinear Magnetization Dynamics in Nanosystems, Elsevier, Oxford, 2009, http://dx.doi.org/10.1016/B978-0-08-044316-4.X0001-1.

[11] X.Z. Yu, Y. Onose, N. Kanazawa, J.H. Park, J.H. Han, Y. Matsui, N. Nagaosa, . Tokura, Real-space observation of a two-dimensional skyrmion crystal, Nature 465 (2010) 901, http://dx.doi.org/10.1038/nature09124.

[12] O.M. Volkov, V.P. Kravchuk, D.D. Sheka, F.G. Mertens, Y. Gaididei, Periodic magnetic structures generated by spin polarized currents in nanostripes, Appl. Phys. Lett. 103 (2013) 222401, http://dx.doi.org/10.1063/1.4831748.

[13] V.P. Kravchuk, O.M. Volkov, D.D. Sheka, Y. Gaididei, Periodic magnetization structures generated by transverse spin current in magnetic nanowires, Phys. Rev. B 87 (2013) 224402, http://dx.doi.org/10.1103/PhysRevB.87.224402.

[14] A.O. Leon, M.G. Clerc, S. Coulibaly, Dissipative structures induced by spin-transfer torques in nanopillars, Phys. Rev. E 89 (2014) 022908, http://dx.doi.org/10.1103/PhysRevE.89.022908.

[15] I.V. Barashenkov, M.M. Bogdan, V.I. Korobov, Stability diagram of the phase-locked solitons in the parametrically driven, damped nonlinear Schrödinger equation, Europhys. Lett. 15 (1991) 113.

[16] A.O. Leon, M.G. Clerc, Spin-transfer-driven nano-oscillators are equivalent to parametric resonators, Phys. Rev. B 91 (2015) 014411, http://dx.doi.org/10.1103/PhysRevB.91.014411.

[17] J. Shibata, G. Tatara, H. Kohno, A brief review of field- and current-driven domain-wall motion, J. Phys. D: Appl. Phys. 44 (2011) 384004, http://dx.doi.org/10.1088/0022-3727/44/38/384004.

[18] S.S.P. Parkin, M. Hayashi, L. Thomas, Magnetic domain-wall racetrack memory, Science 320 (2008) 190, http://dx.doi.org/10.1126/science.1145799.

[19] E. Berrios-Caro, M.G. Clerc, A.O. Leon, Flaming 2π-kinks in parametrically driven systems, Phys. Rev. E 94 (2016) 052217, http://dx.doi.org/10.1103/PhysRevE.94.052217.

[20] Y. Zhang, X. Zhang, N. Vernier, Z. Zhang, G. Agnus, J.-R. Coudevylle, X. Lin, Y. Zhang, Y.-G. Zhang, W. Zhao, D. Ravelosona, Domain-wall motion driven by Laplace pressure in Co - Fe - B / MgO nanodots with perpendicular anisotropy, Phys. Rev. Appl. 9 (2018) 064027, http://dx.doi.org/10.1103/PhysRevApplied.9.064027.

[21] D. Berkov, N. Gorn, Transition from the macrospin to chaotic behavior by a spin-torque driven magnetization precession of a square nanoelement, Phys. Rev. B 71 (2005) 052403, http://dx.doi.org/10.1103/PhysRevB.71.052403.

[22] J. Bragard, H. Pleiner, O.J. Suarez, P. Vargas, J.A.C. Gallas, D. Laroze, Chaotic dynamics of a magnetic nanoparticle, Phys. Rev. E 84 (2011) 037202, http://dx.doi.org/10.1103/PhysRevE.84.037202.

[23] A.M. Cabanas, M.G. Clerc, D. Laroze, A.O. Leon, Chaotic patterns and localized states in spin valves, J. Magn. Magn. 476 (2019) 589, http://dx.doi.org/10.1016/j.jmmm.2019.01.027.

[24] J.A. Vélez, J. Bragard, L.M. Pérez, A.M. Cabanas, O.J. Suarez, D. Laroze, H.L. Mancini, Periodicity characterization of the nonlinear magnetization dynamics, Chaos 30 (2020) 093112, http://dx.doi.org/10.1063/5.0006018.

[25] Y. Shiota, T. Maruyama, T. Nozaki, T. Shinjo, M. Shiraishi, Y. Suzuki, Voltage-assisted magnetization switching in ultrathin $Fe_{80}Co_{20}$ alloy layers, Appl. Phys. Express 2 (2009) 063001, http://dx.doi.org/10.1143/APEX.2.063001.

[26] Y. Suzuki, H. Kubota, A. Tulapurkar, T. Nozaki, Spin control by application of electric current and voltage in FeCo|MgO junctions, Phil. Trans. R. Soc. A 369 (2011) 3658, http://dx.doi.org/10.1098/rsta.2011.0190.

[27] T. Nozaki, Y. Shiota, S. Miwa, S. Murakami, F. Bonell, S. Ishibashi, H. Kubota, K. Yakushiji, T. Saruya, A. Fukushima, S. Yuasa, T. Shinjo, Y. Suzuki, Electric-field-induced ferromagnetic resonance excitation in an ultrathin ferromagnetic metal layer, Nat. Phys. 8 (2012) 491, http://dx.doi.org/10.1038/nphys2298.

[28] S. Kanai, M. Yamanouchi, S. Ikeda, Y. Nakatani, F. Matsukura, H. Ohno, Electric field-induced magnetization reversal in a perpendicular-anisotropy CoFeB-MgO magnetic tunnel junction, Appl. Phys. Lett. 101 (2012) 122403, http://dx.doi.org/10.1063/1.4753816.

[29] J. Zhu, J.A. Katine, G.E. Rowlands, Y.J. Chen, Z. Duan, J.G. Alzate, P. Upadhyaya, J. Langer, P.K. Amiri, K.L. Wang, I.N. Krivorotov, Voltage-induced ferromagnetic resonance in magnetic tunnel junctions, Phys. Rev. Lett. 108 (2012) 197203, http://dx.doi.org/10.1103/PhysRevLett.108.197203.

[30] D. Chiba, M. Sawicki, Y. Nishitani, Y. Nakatani, F. Matsukura, H. Ohno, Magnetization vector manipulation by electric fields, Nat. Lett. 455 (2008) 515, http://dx.doi.org/10.1038/nature07318.

[31] A.O. Leon, A.B. Cahaya, G.E.W. Bauer, Voltage control of rare-earth magnetic moments at the magnetic-insulator metal interface, Phys. Rev. Lett. 120 (2018) 027201, http://dx.doi.org/10.1103/PhysRevLett.120.027201.

[32] A.O. Leon, G.E.W. Bauer, Voltage- and temperature-dependent rare-earth dopant contribution to the interfacial magnetic anisotropy, J. Phys.: Condens. Matter 32 (2020) 404004, http://dx.doi.org/10.1088/1361-648x/ab997c.

[33] T. Nozaki, T. Yamamoto, S. Miwa, M. Tsujikawa, M. Shirai, S. Yuasa, Y. Suzuki, Recent progress in the voltage-controlled magnetic anisotropy effect and the challenges faced in developing voltage-torque MRAM, Micromachines 10 (2019) 327, http://dx.doi.org/10.3390/mi10050327.

[34] T. Chiba, T. Komine, Voltage-driven magnetization switching via Dirac magnetic anisotropy and spin–orbit torque in topological-insulator-based magnetic heterostructures, Phys. Rev. Appl. 14 (2020) 034031, http://dx.doi.org/10.1103/PhysRevApplied.14.034031.

[35] R. Verba, M. Carpentieri, G. Finocchio, V. Tiberkevich, A. Slavin, Amplification and stabilization of large-amplitude propagating spin waves by parametric pumping, Appl. Phys. Lett. 112 (2018) 042402, http://dx.doi.org/10.1063/1.5019357.

[36] R. Verba, V. Tiberkevich, I. Krivorotov, A. Slavin, Parametric excitation of spin waves by voltage-controlled magnetic anisotropy, Phys. Rev. Appl. 1 (2014) 044006, http://dx.doi.org/10.1103/PhysRevApplied.1.044006.

[37] R. Verba, M. Carpentieri, G. Finocchio, V. Tiberkevich, A. Slavin, Excitation of propagating spin waves in ferromagnetic nanowires by microwave voltage-controlled magnetic anisotropy, Sci. Rep. 6 (2016) 25018, http://dx.doi.org/10.1038/srep25018.

[38] Y.-J. Chen, H.K. Lee, R. Verba, J.A. Katine, I. Barsukov, V. Tiberkevich, J.Q. Xiao, A.N. Slavin, I.N. Krivorotov, Parametric resonance of magnetization excited by electric field, Nano Lett. 17 (2017) 572, http://dx.doi.org/10.1021/acs.nanolett.6b04725.

[39] B. Rana, Y. Fukuma, K. Miura, H. Takahashi, Y. Otani, Excitation of coherent propagating spin waves in ultrathin CoFeB film by voltage-controlled magnetic anisotropy, Appl. Phys. Lett. 111 (2017) 052404, http://dx.doi.org/10.1063/1.4990724.

[40] R. Verba, M. Carpentieri, G. Finocchio, V. Tiberkevich, A. Slavin, Excitation of spin waves in an in-plane-magnetized ferromagnetic nanowire using voltage-controlled magnetic anisotropy, Phys. Rev. Appl. 7 (2017) 064023, http://dx.doi.org/10.1103/PhysRevApplied.7.064023.

[41] A.O. Leon, M.G. Clerc, D. Altbir, Dissipative magnetic breathers induced by time-modulated voltages, Phys. Rev. E 98 (2018) 062213, http://dx.doi.org/10.1103/PhysRevE.98.0622133.

[42] M.A. García-Ñustes, F.R. Humire, A.O. Leon, Self-organization in the one-dimensional Landau-Lifshitz-Gilbert-Slonczewski equation with non-uniform anisotropy fields, Commun. Nonlinear Sci. Numer. Simul. 96 (2021) 105674, http://dx.doi.org/10.1016/j.cnsns.2020.105674.

[43] H. Nomura, T. Furuta, K. Tsujimoto, Y. Kuwabiraki, F. Peper, E. Tamura, S. Miwa, M. Goto, R. Nakatani, Y. Suzuki, Reservoir computing with dipole-coupled nanomagnets, Japan. J. Appl. Phys. 58 (2019) 070901, http://dx.doi.org/10.7567/1347-4065/ab2406.

[44] A. Pikovsky, A. Politi, Lyapunov Exponents: A Tool to Explore Complex Dynamics, Cambridge University Press, Cambridge, 2016.

[45] P. Bruno, Tight-binding approach to the orbital magnetic moment and magnetocrystalline anisotropy of transition-metal monolayers, Phys. Rev. B 39 (1989) 865 (R), http://dx.doi.org/10.1103/PhysRevB.39.865.

[46] L.D. Landau, E.M. Lifshitz, Mechanics: Volume 1, in: Course of Theoretical Physics S, Editorial Mir Moscu.

[47] A. Gomel, J.M. Boyer, C. Metayer, J.R. Tredicce, Extreme events in lasers with modulation of the field polarization, Adv. Condens. Matter Phys. 2019 (2019) 7632852, http://dx.doi.org/10.1155/2019/7632852.